RADIATION RESEARCH **170**, 224–234 (2008)
0033-7587/08 $15.00

Terahertz Radiation Increases Genomic Instability in Human Lymphocytes

Avital Korenstein-Ilan,[a] Alexander Barbul,[a] Pini Hasin,[a] Alon Eliran,[b] Avraham Gover[b] and Rafi Korenstein[a,1]

[a] *Department of Physiology and Pharmacology, Faculty of Medicine, and* [b] *Department of Electrical Engineering – Physical Electronics, Faculty of Engineering, Tel-Aviv University, 69978 Tel-Aviv, Israel*

Korenstein-Ilan, A., Barbul, A., Hasin, P., Eliran, A., Gover, A. and Korenstein, R. Terahertz Radiation Increases Genomic Instability in Human Lymphocytes. *Radiat. Res.* 170, 224–234 (2008).

Terahertz radiation is increasingly being applied in new and evolving technologies applied in areas such as homeland security and medical imaging. Thus a timely assessment of the potential hazards and health effects of occupational and general population exposure to THz radiation is required. We applied continuous-wave (CW) 0.1 THz radiation (0.031 mW/cm^2) to dividing lymphocytes for 1, 2 and 24 h and examined the changes in chromosome number of chromosomes 1, 10, 11 and 17 and changes in the replication timing of their centromeres using interphase fluorescence *in situ* hybridization (FISH). Chromosomes 11 and 17 were most vulnerable (about 30% increase in aneuploidy after 2 and 24 h of exposure), while chromosomes 1 and 10 were not affected. We observed changes in the asynchronous mode of replication of centromeres 11, 17 and 1 (by 40%) after 2 h of exposure and of all four centromeres after 24 h of exposure (by 50%). It is speculated that these effects are caused by radiation-induced low-frequency collective vibrational modes of proteins and DNA. Our results demonstrate that exposure of lymphocytes *in vitro* to a low power density of 0.1 THz radiation induces genomic instability. These findings, if verified, may suggest that such exposure may result in an increased risk of cancer.

INTRODUCTION

Terahertz radiation lies at the interface between the infrared and the microwave regions of electromagnetic spectrum, typically defined as the frequency range 100 GHz–10 THz (or 30 μm–3 mm in wavelength). The THz region was a previously underused range of the electromagnetic spectrum, because of a lack of suitable sources and detectors. Progress over the last 10 years in laser and semiconductor technology has enabled the use of this spectral region with an emphasis in applications in sensing (*1, 2*) and communications (*3*) with unique applications in screening for weapons, explosives and biohazards as well as in medical imaging.

This non-ionizing radiation is of particular interest because it has been suggested to excite low-frequency bond vibrations, crystalline phonon vibrations, hydrogen-bonding stretches, and torsion vibrations in important biological molecules such as DNA (*4–6*). Very little is known of the effects of THz radiation on biological systems and about potential damages that could be induced after the absorption of this radiation by living cells (*7–9*). Despite the fact that the public is not yet widely exposed to THz radiation, due to the present state of the technology, a timely assessment of potential hazards and health effects after occupational and general population exposure to THz radiation is needed.

In recent years the public has been increasingly exposed to non-ionizing radiation of the microwave region (mobile phone communication), and much apprehension has been expressed about potential health effects, with cancer being the main concern (*10*). The etiology of cancer has not been fully elucidated, but it is accepted that both genetic (*11*) and epigenetic (*12*) mechanisms are involved. We and others have demonstrated that two basic characteristics of the cell, DNA replication and chromosomal segregation, are disrupted at the onset of carcinogenesis, reflecting increased genomic instability [(*13–17*) references therein]. As a result, there is loss of the normal pattern of replication of the centromeres, the chromosome's moving component (*18*), and the integrity of the diploid human chromosomal complement is compromised, leading to aneuploidy.

We explored the genetic and epigenetic consequences of exposing human peripheral lymphocytes to low-intensity CW 0.1 THz radiation by using FISH to analyze the number of chromosomes present [by counting the centromeric signals; (*18*) and references therein] and by applying the FISH replication assay (*19, 20*).

METHODS

Cultures

Lymphocytes were isolated by UNI-SEP$_{maxi}$ (NovaMed Ltd., Jerusalem, Israel. Catalog no. U-10) from 20 ml of whole blood obtained by vacu-

[1] Address for correspondence: Department of Physiology and Pharmacology, Faculty of Medicine, Tel-Aviv University, 69978 Tel-Aviv, Israel; e-mail: korens@post.tau.ac.il.

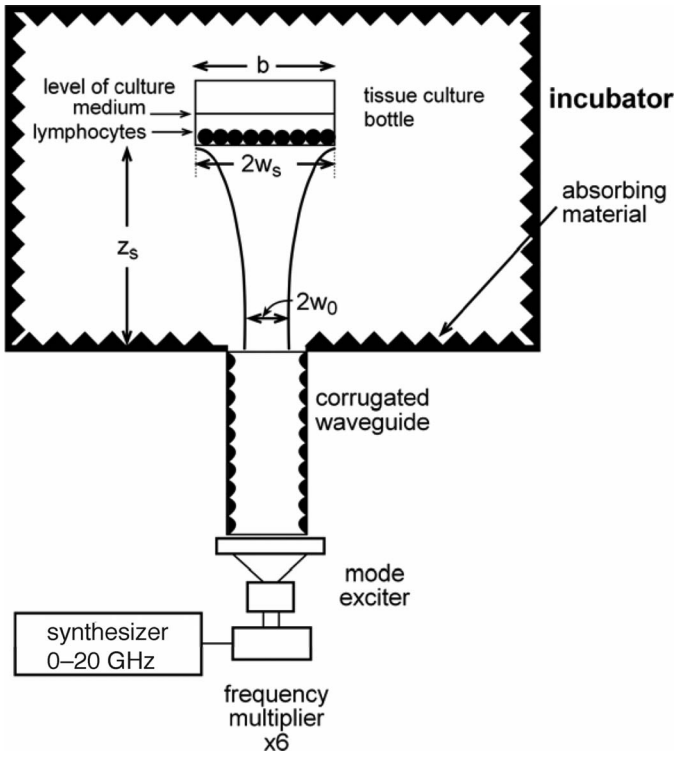

FIG. 1. Schematic block diagram of the exposure setup for 0.1 THz CW radiation. 16.6 GHz radiation produced by a CW generator is multiplied sixfold by a frequency multiplier unit, fed into a special mode exciter, and transmitted into a cylindrical corrugated waveguide. The 0.1 THz radiation emerging from the waveguide has a waist spot diameter of $2w_0$, propagates a distance of z_s reaching the bottom of the tissue culture flask, where the bean waist expands twofold to a size of $2w_s$. The power density flux of 0.031 mW/cm^2 hits the very thin layer of lymphocytes (~0.003 cm) at the bottom of a 0.2-cm-deep layer of culture fluid covering an area of 23 cm^2. The incident 0.1 THz radiation is attenuated to its 1/e intensity at a water thickness of 0.013 cm.

puncture into heparin-containing vacutainers from nine male volunteers ages 24 to 59 (average 34 ± 13). The protocols were approved by the institutional review board (Helsinki committee) of Tel-Aviv University. Lymphocytes were counted and seeded at 0.5×10^6 cells/ml in growth medium. Five milliliters of the cell suspension was placed in each of seven 25-cm^2 flasks (catalog no. TP-9025, TPP, Switzerland) placed horizontally in an incubator at 37°C and a humidified atmosphere of 95% air/5% CO_2 for 1–6 h before exposure. The growth medium consisted of RPMI-1640 medium (catalog no. 01-100-1A), 20% inactivated FCS (catalog no. 04-121-1A), 1% antibiotics (catalog no. 03-032-1C), 3% PHA-M (catalog no. 12-006-1H), all from Biological Industries, Israel, and 0.2% heparin (5000 U/ml, Evans-Promedico, Israel).

Exposure Setup

Figure 1 shows a schematic block diagram of the exposure setup. It consists of an exposure cell, an RF generator, and means to measure the RF power and the culture temperature. The culture flask (width = 4.1 cm, length = 5.6 cm) was placed at a distance $z_s = 28$ cm from the end of a cylindrical waveguide that was designed for bottom illumination.

The millimeter-wave source of radiation consisted of a CW generator (HP8620C) and a sixfold frequency multiplier (AMC-10-00000, Millitech) yielding a 100 GHz CW radiation. The cylindrical waveguide was a special low-loss over-moded corrugated waveguide that was fed from the frequency multiplier unit a special mode exciter (tapered feed; Gycom, Russia). The waveguide was a corrugated aluminum cylinder with an inner diameter $2R_w$ of 3.8 cm and a length of 33.4 cm. This type of waveguide supports a linearly polarized fundamental hybrid mode (EH_{11}) that can excite the fundamental free-space diffraction Gaussian mode with close to 100% efficiency (*21*). The power density distribution of this mode is (*22*)

$$w(z) = w_0(1 + z^2/z_R^2)^{1/2}$$

$$I_{00}(x, y, z) = I_{00}(0, 0, z)e^{-2[x^2+y^2/w^2(z)]}, \quad (1)$$

where z is the vertical distance from the waveguide exit, (x, y) are the transverse coordinates relative to the optical (waveguide) axis; z_R is the Rayleigh length ($z_R = \pi w_0^2/\lambda$) of the radiation beam of wavelength λ with beam waist spot diameter $2w_0$. The beam waist is located at the waveguide exit, and its half width is $w_0 = 0.63R_w$ (*21*).

The exposure setup was installed within an incubator to keep it at a constant temperature. The inner walls, ceiling and floor of the incubator were covered with pyramidal radiation-absorbing material (APM9, Hyfral, France) to avoid uncontrolled illumination of the sample due to reflections. The bottom illumination design was chosen to ensure that the lymphocytes that sank to the bottom of the flask would be within the area of absorption of the radiation by the liquid and thus would all be exposed to radiation. The decay of the radiation intensity inside the liquid due to absorption is

$$I(z) = I(z_s^+)e^{-\alpha(z-z_s)}, \quad (2)$$

where z_s is the distance of the sample from the waveguide exit and z_s^+ refers to the inner side (sample side) of the bottom wall of the flask; i.e., $I(z_s^+)$ is the intensity transmitted into the sample flask at any transverse position (x, y). Its transverse variation is given by Eq. (1).

The lymphocytes were exposed uniformly to the same field and power density $[I(z_s^+)]$ assuming they all sank to the bottom of the tissue culture flask in a layer (~30–40 μm) much thinner than the absorption length $1/\alpha$. The transmitted radiant (power) intensity is calculated from the incident intensity using the Fresnel relation $I(z_s^+) = TI(z_s^-)$, where T is the power transmission coefficient from air to the liquid (neglecting the thin polystyrene wall of the flask):

$$T = 1 - R \approx 1 - \left(\frac{n_{\text{water}} - n_{\text{air}}}{n_{\text{water}} + n_{\text{air}}}\right)^2, \quad (3)$$

where R is the power reflection coefficient.

With these assumptions, integrating over the intensity transverse variation (Eq. 1), lymphocytes residing within the absorption depth $1/\alpha$ and within the beam spot radius $w(z_s)$ are illuminated with an average SAR given by

$$\text{SAR} = \alpha\overline{I(z_s^+)}/\rho = \alpha\overline{TI(z_s^-)}/\rho = \alpha T(\eta_{\text{diff}}P_0/ab)/\rho, \quad (4)$$

where ρ is the specific mass of the liquid, P_0 is the total power emitted from the exit of the waveguide, and $\overline{I(z_s)} = \eta_{\text{diff}}P_0/ab$ is the average power density incident on the sample (of dimensions $a \times b$), where

$$\eta_{\text{diff}} = \frac{\iint_{\text{sample}} I_{\text{inc}}(x, y)\, dx\, dy}{\int_{-\infty}^{\infty}\int I_{\text{inc}}(x, y)\, dx\, dy} = \text{erf}\left(\frac{a}{\sqrt{2}w_s}\right)\text{erf}\left(\frac{b}{\sqrt{2}w_s}\right). \quad (5)$$

Numerical Dosimetry

$2w_0$, the beam waist diameter at the waveguide end, is 2.4 cm. $2w_s$, the beam spot diameter at the sample (bottom of flask), is 5 cm (Eq. 1). Substituting all numbers, we find $\eta_{\text{diff}} = 87\%$ (Eq. 5). The generator was set at its maximum output power level of 13 dBm. Taking into account the measured 24% attenuation of the mode exciter, the total illumination power incident on the sample was determined to be $P_{\text{inc}} = \eta_{\text{diff}}P_0 = 1$ mW and the average power density incident at the bottom of the flask is $\overline{I(z_s^-)} = 1$ mW/23cm^2 = 0.043 mW/cm^2.

To calculate the power actually reaching the cells inside the culture

flask, Fresnel refraction from the sample was calculated for the following configuration: $n_{air} = 1$; $n_{polystyrene} = 1.6$; $n_{water} = 3.3$. Due to the low diffraction coefficient of polystyrene, which has an optical thickness much lower than λ, it can be neglected. Refraction and transmission coefficients were found to be (Eq. 3) $R = 29\%$ and $T = 71\%$, respectively. The average power density into the sample was $I_s = \overline{I(z_s^+)} = T \times \overline{I(z_s^-)} = 0.031$ mW/cm^2. Since the cell suspension is comprised mostly of water, the attenuation of the radiation upon penetrating the cell suspension can be attributed to water alone. The attenuation factor of water at 100 GHz is $1/\alpha = 0.013$ cm (*23*), and the specific weight is $\rho = 1$ g/cm^3. Thus the calculated SAR value using Eq. (4) is $\alpha I_s/\rho = 1/0.013 \times 0.031/1 = 2.4$ mW/g.

The power density $I(r)$ was verified to follow a Gaussian distribution (Eq. 1). Thus the power density across the sample stays in the range $0.5I_c < I(r) < I_c$ in a circle 3 cm in diameter around the center of the sample.

Thermal Effects

To ascertain that the effects induced by exposing the cells to 0.1 THz CW radiation were not thermal, we monitored the rise in temperature during exposure. Two fiber-optic temperature sensors (FISO Technologies, Quebec, Canada) were located in the vicinity of the flask bottom, where the cells are concentrated, with one inserted into an irradiated flask and the other inserted into a sham-exposed flask placed in the same incubator but not irradiated (see the next section). The data were recorded every 2.2 s, averaging 1 s per point. The flasks were filled with growth medium and temperature-equilibrated before exposure was initiated. The differences between the two sensors did not exceed 0.3°C throughout the experiment (1–24 h).

Experimental Design

Two flasks, one to be exposed and one to be wrapped in aluminum foil and placed in the exposure setup on a bottom shelf for sham exposure, were set up for each exposure time (1, 2 and 24 h). In addition, one culture was left undisturbed in the regular incubator. It should be noted that the exposure setup is placed in an incubator that does not have a 5% CO_2 atmosphere. Thus, while control samples were undisturbed for the duration of the culturing, the sham-exposed and exposed samples were subject to transfers from one incubator to another and to periods of between 1.5 and 24.5 h of no CO_2 atmosphere. Exposure started after the flasks had been in the exposure system for 30 min to ensure that all lymphocytes sank to the bottom of the flask and were equilibrated to the incubator's temperature. Immediately after the exposure, flasks were returned to the regular CO_2 incubator and grown for a total of 69–72 h at 37°C (all flasks for an experiment were harvested at the same time).

Harvest

Cells were harvested according to standard cytogenetic protocols (*24*). Briefly, after 1 h of colchicine treatment (final concentration 0.2 μg/ml; Biological Industries, Israel; catalog no. 12-003-1C) hypotonic treatment was performed (0.06 *M* KCl at 37°C for 12 min) followed by four washes with fresh cold (−20°C) 3:1 methanol:acetic acid solution (fixative). Nuclear suspensions were stored at −80°C until used for FISH.

FISH

We performed two-color FISH using two probe combinations. We used Vysis Inc. probes recognizing the centromeres of either chromosomes 11 and 17 (catalog nos. 32-130011 and 32-132017, respectively) or chromosomes 1 and 10 (catalog nos. 32-130001 and 32-132010, respectively) with the spectrum orange and spectrum green fluorophores, respectively. We analyzed all nine samples for the levels of aneuploidy, replication timing and asynchrony using the centromeres of chromosomes 11 and 17. Five of these, randomly chosen, were also used for analyzing the centromeres of chromosomes 1 and 10. Nuclear suspensions that had been diluted until they were slightly cloudy were dropped onto two-well slides obtained from Insitus Biotechnologies that were used without any pretreatment. We followed a standard protocol recommended by Insitus Biotechnologies: The probes were diluted 700-fold using DenHyb D001 (Insitus Biotechnologies). Then 5 μl of the probe solution was placed on the marked spot on the slide and covered with 12-mm round silianized cover slips (Insitus Biotechnologies). Co-denaturation of nuclei and probe was performed in a slide moat (model 240000; Boekel Scientific) at 90°C for 6 min, and slides were then transferred to a covered humidified aluminum tray and placed in a 37°C incubator. Slides were post washed between 4 and 8 h later at 78°C for 4 min in each of the post-washing solutions: 0.4× SSC (1× SSC = 150 m*M* NaCl, 15 m*M* sodium citrate) with 0.3% NP40 and 2× SSC and 0.1% NP40. After the excess liquid was drained off, slides were treated with 15 μl of an antifade solution containing 3 μg/ml of 4,6-diamino-2-phenylindole (DAPI) as a counterstain (Vectashield, Vector Labs), covered with glass cover slips, and stored in the dark at −20°C until microscopic analysis.

Analysis

Images were acquired using the Metacyte system (MetaSystems, Altlussheim, Germany), which is a fluorescence object finding and relocation system based on a fully motorized Axioplan2 microscope (Zeiss, Germany), a motorized eight-slide scanning stage (Marzhauser, Germany), a high-resolution CCD camera with chip integration, and a PC equipped with appropriate modules for accurate stage movement and fast image analysis. Metafer 4 is an image analysis software package designed to automatically perform spot counting based on an algorithm (classifier) prepared and optimized by the user. This algorithm takes into account the shape and size of the nuclei as well as the shape, size and relative intensity of the spots counted. To help avoid scoring cells that were unaffected by the mitogenic stimulus of PHA, we restricted our analysis to nuclei with an area greater than 50 μm^2 (the proportion of these cells did not differ significantly between exposed and sham-exposed samples). We also excluded from analysis any nuclei that were nullisomic for either of the two chromosomes studied. Slides were scanned and scored automatically, and the galleries obtained were then corrected manually.

For the analysis of aneuploidy, about 1400 interphase cells (mean 1360 ± 253) were scored for the number of signals representing the number of chromosomes in those cells. The level of aneuploidy is given as the proportion of cells with less than the expected two signals (monosomy) or more than the expected two (multisomy). In Fig. 2, cells from a Metafer gallery are shown that represent a cell with two signals in each of the color channels (panel a) and a cell (panel b) with only one red signal (monosomy) and four green signals (multisomy).

For the analysis of replication timing and asynchrony, about 700 interphase cells (mean 681 ± 73) with two hybridization signals for both centromeres were examined. The shape of the signal was noted and recorded as described previously (*14, 19, 20*). Briefly, signals were categorized as representing unreplicated sequences (single spots, S) or replicated sequences (double dots, D). Each cell was scored as either early replicating (having two already replicated sequences, DD, Fig. 2e), late replicating (having two unreplicated sequences, SS, Fig. 2c), or asynchronous (having one replicated and one as yet unreplicated sequence, SD, Fig. 2d). Most sequences replicate synchronously at distinct time domains during S phase (*14, 19*), with active genes replicating early and silenced or untranscribed loci (such as the centromeres) replicating late. In the cancerous genome, the normal mode of coordinated replication is disrupted and an increased fraction of the cells replicate asynchronously [(*14*) and references within].

We used the Metafer 4 aneuploidy galleries to prepare a file containing the images of the subset of cells to be analyzed. These were analyzed manually based on their replication status by one of us (AKI) according to the signal shapes and the proportion of cells in each category was noted.

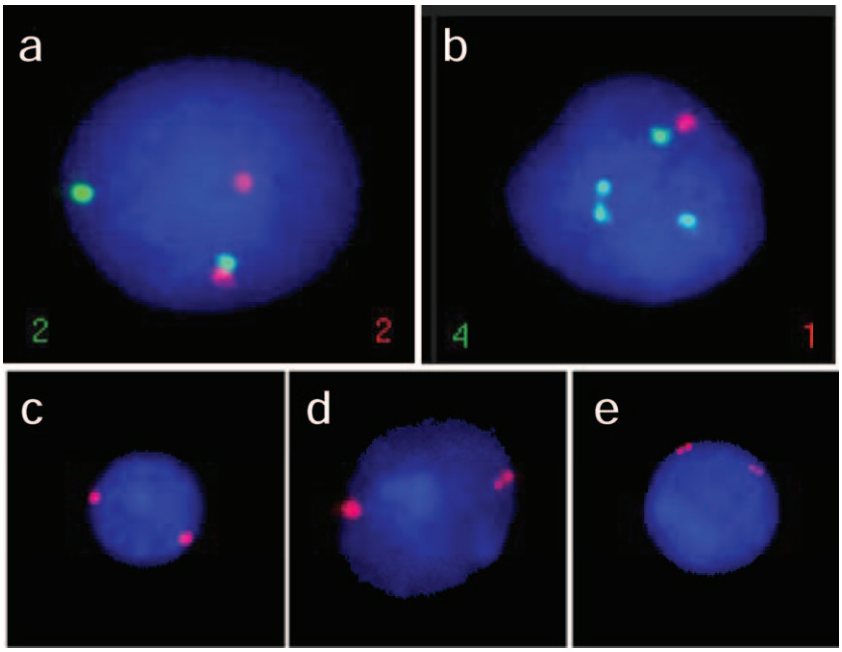

FIG. 2. Representative interphase FISH images of nuclei with genomically stable (panels a, c and e) and genomically unstable cells (panels b and d). The centromeres of chromosomes 11 and 17 are identified using FISH. The nucleus in panel a exhibits two signals for each of the loci tested (red, centromere 11; green, centromere 17), while the one in panel b displays monosomy of centromere 11 (one red signal) and multisomy of centromere 17 (four green signals). The nuclei in panels c–e show the various replication patterns observed. In panels c and e, the two centromeres of chromosome 11 are in the same coordinated replicative state (synchronous replication): panel c: as yet unreplicated sequences, late replication; panel e: both sequences have already replicated, early replication. In panel d one of the centromeres has already been replicated and the other has not yet reached asynchronous replication.

Statistics

Multivariate analysis of variance (MANOVA, SPSS 15.0.1) was used for the statistical analyses. The multivariate general linear model with two fixed factors, THz radiation and blood source (donor ID), was employed. The main effects of the factors on total aneuploidy, multisomy, and late (SS) and asynchronous (SD) cell replication were studied. THz radiation was examined at three times (1, 2 and 24 h) for centromeres 11 and 17 and at two times (2 and 24 h) for centromeres 1 and 10. A large variability between donors was revealed because the blood source was found to be a significant variable ($P < 0.05$) for all chromosomes and effects studied. The exposure was found to be a significant factor for the model in only some of the cases. The reliance of the dependent variables on exposure duration was checked using post hoc Tukey's honestly significant difference (Tukey's HSD) test by comparison of data obtained for 1, 2 and 24 h THz radiation exposure with the respective data from sham-exposed samples.

RESULTS

Human lymphocytes isolated from peripheral blood cells were exposed *in vitro* to 0.1 THz CW radiation, at a low average power density of 0.031 mW/cm^2 in a specially designed exposure setup (Fig. 1). The samples were exposed for 1 (0.11 J/cm^2), 2 (0.22 J/cm^2) or 24 (2.68 J/cm^2) and were harvested together after a total of 69–72 h for cytogenetic analysis. The effect of exposure on the level of aneuploidy of chromosomes 1, 10, 11 and 17 as well as the replication timing and synchrony of the respective centromeres was examined. These chromosomes were selected because they host genes important in tumorigenesis and also implicated in cell cycle control and/or damage response (*HPC1, PTEN, ATM* and p53, respectively). The results are summarized in the tables, which give the numbers of nuclei scored and the numbers and percentages of aberrant nuclei (containing more or less than the expected two signals) or multisomic nuclei (gains) or the number of nuclei with asynchronous or late replication in that population for each of the chromosomes analyzed. In Table 1, the data for the control samples are provided; Tables 2 (centromeres 11 and 17) and 3 (centromeres 1 and 10) summarize the data for chromosomal losses and gains. Tables 4 (centromeres 11 and 17) and 5 (centromeres 1 and 10) summarize the data for the replication timing and asynchrony.

There were no statistically significant differences between sham-exposed and control samples in almost all of the experiments performed (data not shown). Since the sham-exposed samples had undergone the same treatment and handling as the exposed samples, we always compared our exposed and sham-exposed samples. There was no significant difference ($P = 0.2$; $n = 7$) in the proportion of metaphase cells in the exposed and sham-exposed samples, suggesting that exposure did not induce an effect on cell cycling.

TABLE 1
Levels of Aneuploidy (Multisomy and Total) and Replication (Asynchronous and Late) in Control Samples for each Donor

		Centromere 11				Centromere 17					Centromere 11				Centromere 17			
		Multisomy		Total		Multisomy		Total			Asynchronous replication		Late replication		Asynchronous replication		Late replication	
Donor	n_s	n_m	Percent	n_t	Percent	n_m	Percent	n_t	Percent	n_s	n_a	Percent	n_l	Percent	n_a	Percent	n_l	Percent
1	860	18	2.1	67	7.8	15	1.7	82	9.5	606	90	14.9	496	81.8	67	11.1	522	86.1
2	1167	15	1.3	114	9.8	24	2.1	140	12.0	770	86	11.2	657	85.3	72	9.4	679	88.2
3	932	24	2.6	112	12.0	25	2.7	87	9.3	629	76	12.1	540	85.9	84	13.4	519	82.5
4	890	22	2.5	110	12.4	38	4.3	152	17.1	741	101	13.6	625	84.3	109	14.7	605	81.6
5	1273	20	1.6	120	9.4	31	2.4	155	12.2	739	65	8.8	659	89.2	67	9.1	640	86.6
6	1147	25	2.2	103	9.0	21	1.8	123	10.7	707	96	13.6	600	84.9	88	12.4	600	84.9
7	1384	11	0.8	146	10.5	23	1.7	198	14.3	667	94	14.1	553	82.9	105	15.7	538	80.7
8	1515	16	1.1	85	5.6	28	1.8	156	10.3	650	95	14.6	533	82.0	105	16.2	516	79.4
9	1527	20	1.3	99	6.5	21	1.4	152	10.0	644	50	7.8	583	90.5	58	9.0	577	89.6

		Centromere 1				Centromere 10					Centromere 1				Centromere 10			
		Multisomy		Total		Multisomy		Total			Asynchronous replication		Late replication		Asynchronous replication		Late replication	
Donor	n_s	n_m	Percent	n_t	Percent	n_m	Percent	n_t	Percent	n_s	n_a	Percent	n_l	Percent	n_a	Percent	n_l	Percent
1	1540	32	2.1	174	11.3	36	2.3	177	11.5	690	126	18.3	522	75.7	117	17.0	557	80.7
3	1126	59	5.2	152	13.5	33	2.9	158	14.0	766	186	24.3	515	67.2	100	13.1	652	85.1
5	1525	65	4.3	225	14.8	51	3.3	203	13.3	661	173	26.2	392	59.3	62	9.4	594	89.9
6	1487	113	7.6	223	15.0	96	6.5	169	11.4	640	134	20.9	435	68.0	124	19.4	487	76.1
9	1572	65	4.1	147	9.4	43	2.7	113	7.2	654	131	20.0	460	70.3	140	21.4	463	70.8

Notes. The numbers of nuclei scored (n_s) are given for chromosomes 11 and 17 together and for chromosomes 1 and 10 together since double hybridization was performed. n_t and n_m are the number of total aneuploid and multisomic nuclei, respectively; n_a and n_l are the number of asynchronous and late replication nuclei, respectively.

Changes in Aneuploidy Levels

For centromeres 11 and 17, the exposure of cells to THz radiation was found to be a statistically significant source of variance in aneuploidy, $P < 0.001$ and $P < 0.003$, and in multisomy, $P < 0.005$ and $P < 0.001$, respectively. THz radiation was found to induce significant changes in the total aneuploidy level of chromosome 1 ($P < 0.014$) but not in the multisomy ($P = 0.357$). For centromere 10, no significant changes were found after exposure for either aneuploidy ($P = 0.884$) or multisomy ($P = 0.468$). Pairwise comparisons showed no statistically significant changes in the levels of aneuploidy after exposure of the samples to 0.1 THz radiation for 1 h for either chromosome 11 or 17 (Fig. 3). However, increasing the exposure time to 2 h caused an increase in the level of aneuploidy of chromosomes 11 and 17 by 1.35 ± 0.37-fold ($P = 0.015$) and 1.22 ± 0.25-fold ($P = 0.135$), respectively. This increase was mainly due to an elevation in chromosomal gains by 1.71 ± 0.43-fold ($P = 0.009$) and 2.13 ± 0.59-fold ($P = 0.003$) for chromosomes 11 and 17, respectively (Fig. 4). After 24 h exposure, there was a significant increase in the level of total aneuploidy of chromosome 11 (by 1.30 ± 0.27-fold, $P = 0.031$) and chromosome 17 (by 1.32 ± 0.23-fold, $P = 0.010$). This increase was not reflected in increased gains of chromosome 11 ($P = 0.4$; Fig. 4) as opposed to chromosome 17 ($P = 0.050$; Fig. 4). The aneuploidy level of chromosome 1 after exposure of cells to radiation for 2 and 24 h, increased by 1.19 ± 0.14-fold ($P = 0.038$) and 1.12 ± 0.11-fold ($P = 0.159$), respectively. No statistical significance was observed for any of the exposures for chromosome 10.

Changes in the Level of Replication Timing and Coordination

For centromeres 11 and 17, the exposure of cells to THz radiation was found to be a statistically significant source of variance in late replication ($P < 0.021$ and $P < 0.0005$, respectively) as well as in asynchronous replication ($P < 0.001$ and $P < 0.0005$, respectively). Exposure to THz radiation also led to increased asynchronous replication of centromeres 1 and 10 ($P < 0.0005$ and $P < 0.019$, respectively). However, the exposure of the cells to THz radiation led to statistically significant changes in late replication for centromere 1 ($P < 0.014$) but not for centromere 10 ($P = 0.103$).

Similar to the changes in the level of aneuploidy, there were no significant changes for chromosome 11 or 17 in the level of either replication timing or synchrony after 1 h of exposure. Statistically significant increases in the level of asynchronous replication of centromeres 1, 11 and 17 were observed after 2 h of radiation exposure (Fig. 5). The level of asynchronous replication increased by 1.35 ± 0.31-fold for centromere 11 ($P = 0.035$), by 1.46 ± 0.37-fold for centromere 17 ($P = 0.003$), and by 1.52 ± 0.18-fold

TABLE 2
Aneuploidy and Multisomy for Chromosomes 11 and 17 after Exposure to 0.1 THz Radiation for Different Times for each Donor

			Centromere 11				Centromere 17						Centromere 11				Centromere 17			
			Multisomy		Total		Multisomy		Total				Multisomy		Total		Multisomy		Total	
Donor		n_s	n_m	Percent	n_t	Percent	n_m	Percent	n_t	Percent		n_s	n_m	Percent	n_t	Percent	n_m	Percent	n_t	Percent
1	Sham 1 h	899	21	2.3	69	7.7	16	1.8	78	8.7	Exposed 1 h	966	26	2.7	116	12.0	20	2.1	156	16.1
2		1039	23	2.2	95	9.1	42	4.0	147	14.1		948	26	2.7	96	10.1	26	2.7	121	12.8
3		1299	31	2.4	112	8.6	47	3.6	175	13.5		1189	39	3.3	115	9.7	13	1.1	92	7.7
4		1472	46	3.1	203	13.8	81	5.5	259	17.6		883	40	4.5	123	13.9	74	8.4	186	21.1
5		1356	26	1.9	137	10.1	25	1.8	181	13.3		1278	22	1.7	95	7.4	30	2.3	134	10.5
6		1641	19	1.2	145	8.8	29	1.8	195	11.9		1538	14	0.9	139	9.0	29	1.9	180	11.7
7		1279	13	1.0	107	8.4	17	1.3	149	11.6		1536	32	2.1	201	13.1	30	2.0	235	15.3
8		1217	30	2.5	112	9.2	49	4.0	178	14.6		1553	23	1.5	133	8.6	44	2.8	245	15.8
9		1550	17	1.1	115	7.4	23	1.5	181	11.7		1549	25	1.6	123	7.9	23	1.5	167	10.8
1	Sham 2 h	1217	22	1.8	125	10.3	20	1.6	144	11.8	Exposed 2 h	1403	34	2.4	163	11.6	39	2.8	168	12.0
2		1071	17	1.6	79	7.4	18	1.7	107	10.0		1110	40	3.6	168	15.1	49	4.4	151	13.6
3		1375	39	2.8	115	8.4	27	2.0	163	11.9		1531	52	3.4	166	10.8	76	5.0	240	15.7
4		1770	68	3.8	212	12.0	95	5.4	229	12.9		1037	82	7.9	182	17.6	84	8.1	221	21.3
5		1248	18	1.4	133	10.7	19	1.5	188	15.1		1544	33	2.1	135	8.7	37	2.4	187	12.1
6		785	9	1.1	58	7.4	7	0.9	74	9.4		1305	23	1.8	121	9.3	37	2.8	176	13.5
7		1401	18	1.3	159	11.3	17	1.2	164	11.7		1521	24	1.6	164	10.8	28	1.8	216	14.2
8		1236	17	1.4	79	6.4	19	1.5	167	13.5		2036	57	2.8	201	9.9	73	3.6	308	15.1
9		1495	13	0.9	82	5.5	14	0.9	164	11.0		1518	29	1.9	134	8.8	31	2.0	180	11.9
1	Sham 24 h	1276	37	2.9	103	8.1	37	2.9	136	10.7	Exposed 24 h	1407	33	2.3	197	14.0	37	2.6	206	14.6
2		988	14	1.4	90	9.1	20	2.0	121	12.2		1903	70	3.7	271	14.2	84	4.4	381	20.0
3		1406	25	1.8	102	7.3	30	2.1	138	9.8		1413	47	3.3	143	10.1	81	5.7	212	15.0
4		1060	29	2.7	149	14.1	41	3.9	189	17.8		1198	44	3.7	136	11.4	61	5.1	184	15.4
5		1552	25	1.6	131	8.4	22	1.4	193	12.4		1009	16	1.6	114	11.3	32	3.2	155	15.4
6		1314	11	0.8	129	9.8	19	1.4	148	11.3		938	11	1.2	105	11.2	34	3.6	153	16.3
7		1571	21	1.3	149	9.5	33	2.1	237	15.1		1539	38	2.5	199	12.9	39	2.5	257	16.7
8		1126	21	1.9	75	6.7	28	2.5	136	12.1		1170	20	1.7	102	8.7	24	2.1	180	15.4
9		1492	25	1.7	107	7.2	32	2.1	144	9.7		1576	34	2.2	123	7.8	50	3.2	214	13.6

Note. The numbers of nuclei scored (n_s) are given for chromosomes 11 and 17 together since double hybridization was performed. n_t and n_m are the number of total aneuploid and multisomic nuclei, respectively.

TABLE 3
Aneuploidy and Multisomy for Chromosomes 1 and 10 after Exposure to 0.1 THz Radiation for Different Times for each Donor

			Centromere 1				Centromere 10						Centromere 1				Centromere 10			
			Multisomy		Total		Multisomy		Total				Multisomy		Total		Multisomy		Total	
Donor		n_s	n_m	Percent	n_t	Percent	n_m	Percent	n_t	Percent		n_s	n_m	Percent	n_t	Percent	n_m	Percent	n_t	Percent
1	Sham 2 h	1547	25	1.6	171	11.1	23	1.5	184	11.9	Exposed 2 h	1554	73	4.7	210	13.5	43	2.8	132	8.5
3		1659	56	3.4	199	12.0	38	2.3	313	18.9		1566	55	3.5	193	12.3	31	2.0	270	17.2
5		1556	35	2.2	161	10.3	27	1.7	103	6.6		1537	39	2.5	222	14.4	38	2.5	274	17.8
6		1072	69	6.4	137	12.8	38	3.5	106	9.9		1513	82	5.4	219	14.5	60	4.0	156	10.3
9		1522	35	2.3	158	10.4	22	1.4	98	6.4		1389	63	4.5	166	12.0	36	2.6	106	7.6
1	Sham 24 h	1716	22	1.3	199	11.6	17	1.0	180	10.5	Exposed 24 h	1549	54	3.5	208	13.4	44	2.8	185	11.9
3		1556	35	2.2	176	11.3	23	1.5	265	17.0		1579	39	2.5	184	11.7	18	1.1	133	8.4
5		1028	35	3.4	136	13.2	38	3.7	114	11.1		1283	59	4.6	209	16.3	50	3.9	202	15.7
6		1527	67	4.4	218	14.3	59	3.9	202	13.2		1529	72	4.7	218	14.3	39	2.6	127	8.3
9		1525	61	4.0	151	9.9	44	2.9	117	7.7		1237	50	4.0	149	12.0	39	3.2	123	9.9

Note. The numbers of nuclei scored (n_s) are given for chromosomes 1 and 10 together since double hybridization was performed. n_t and n_m are the number of total aneuploid and multisomic nuclei, respectively.

TABLE 4
Asynchronous and Late Replication for Chromosomes 11 and 17 after Exposure to 0.1 THz Radiation for Different Times for each Donor

			Centromere 11				Centromere 17						Centromere 11				Centromere 17			
			Asynchronous replication		Late replication		Asynchronous replication		Late replication				Asynchronous replication		Late replication		Asynchronous replication		Late replication	
Donor		n_s	n_a	Percent	n_l	Percent	n_a	Percent	n_l	Percent		n_s	n_a	Percent	n_l	Percent	n_a	Percent	n_l	Percent
1	Sham 1 h	619	124	20.0	480	77.5	89	14.4	510	82.4	Exposed 1 h	653	105	16.1	526	80.6	106	16.2	527	80.7
2		705	72	10.2	619	87.8	37	5.2	662	93.9		622	105	16.9	483	77.7	53	8.5	560	90.0
3		668	115	17.2	517	77.4	71	10.6	579	86.7		619	118	19.1	487	78.7	113	18.3	490	79.2
4		626	84	13.4	506	80.8	111	17.7	459	73.3		597	150	25.1	428	71.7	145	24.3	410	68.7
5		616	77	12.5	520	84.4	69	11.2	529	85.9		921	92	10.0	821	89.1	86	9.3	828	89.9
6		666	75	11.3	576	86.5	86	12.9	550	82.6		654	119	18.2	526	80.4	129	19.7	501	76.6
7		660	66	10.0	577	87.4	86	13.0	555	84.1		632	80	12.7	537	85.0	91	14.4	529	83.7
8		617	84	13.6	522	84.6	89	14.4	499	80.9		600	134	22.3	435	72.5	115	19.2	460	76.7
9		664	104	15.7	535	80.6	116	17.5	528	79.5		643	89	13.8	535	83.2	111	17.3	510	79.3
1	Sham 2 h	603	82	13.6	507	84.1	94	15.6	491	81.4	Exposed 2 h	672	143	21.3	515	76.6	88	13.1	577	85.9
2		697	103	14.8	555	79.6	66	9.5	615	88.2		752	150	19.9	583	77.5	116	15.4	627	83.4
3		650	119	18.3	479	73.7	70	10.8	568	87.4		865	254	29.4	572	66.1	177	20.5	660	76.3
4		709	121	17.1	555	78.3	106	15.0	560	79.0		606	177	29.2	408	67.3	153	25.2	423	69.8
5		658	74	11.2	580	88.1	58	8.8	596	90.6		676	97	14.3	569	84.2	102	15.1	566	83.7
6		682	94	13.8	573	84.0	97	14.2	540	79.2		699	108	15.5	583	83.4	148	21.2	518	74.1
7		674	96	14.2	570	84.6	105	15.6	552	81.9		651	108	16.6	525	80.6	127	19.5	511	78.5
8		647	109	16.8	521	80.5	103	15.9	518	80.1		958	119	12.4	825	86.1	141	14.7	802	83.7
9		656	65	9.9	583	88.9	69	10.5	576	87.8		659	108	16.4	534	81.0	117	17.8	515	78.1
1	Sham 24 h	606	94	15.5	494	81.5	94	15.5	495	81.7	Exposed 24 h	919	180	19.6	719	78.2	170	18.5	720	78.3
2		607	108	17.8	482	79.4	84	13.8	507	83.5		812	168	20.7	614	75.6	139	17.1	643	79.2
3		677	94	13.9	548	80.9	98	14.5	550	81.2		678	159	23.5	500	73.7	145	21.4	520	76.7
4		789	147	18.6	553	70.1	142	18.0	519	65.8		672	197	29.3	442	65.8	174	25.9	470	69.9
5		695	42	6.0	649	93.4	44	6.3	647	93.1		675	108	16.0	555	82.2	124	18.4	529	78.4
6		953	171	17.9	749	78.6	168	17.6	730	76.6		625	137	21.9	472	75.5	126	20.2	465	74.4
7		658	60	9.1	578	87.8	76	11.6	567	86.2		616	90	14.6	518	84.1	117	19.0	474	76.9
8		662	114	17.2	505	76.3	117	17.7	500	75.5		650	141	21.7	481	74.0	146	22.5	464	71.4
9		669	49	7.3	615	91.9	70	10.5	590	88.2		671	70	10.4	594	88.5	98	14.6	559	83.3

Note. The numbers of nuclei studied (n_s) are given for chromosomes 11 and 17 together since double hybridization was performed. n_a and n_l are the number of asynchronous and late replication nuclei, respectively.

TABLE 5
Asynchronous and Late Replication for Chromosomes 1 and 10 after Exposure to 0.1 THz Radiation for Different Times for each Donor

			Centromere 1				Centromere 10						Centromere 1				Centromere 10			
			Asynchronous replication		Late replication		Asynchronous replication		Late replication				Asynchronous replication		Late replication		Asynchronous replication		Late replication	
Donor		n_s	n_a	Percent	n_l	Percent	n_a	Percent	n_l	Percent		n_s	n_a	Percent	n_l	Percent	n_a	Percent	n_l	Percent
1	Sham 2 h	659	146	22.2	489	74.2	82	12.4	573	86.9	Exposed 2 h	701	202	28.8	448	63.9	92	13.1	601	85.7
3		661	98	14.8	539	81.5	81	12.3	567	85.8		675	188	27.9	452	67.0	102	15.1	561	83.1
5		636	132	20.8	459	72.2	86	13.5	537	84.4		645	166	25.7	448	69.5	64	9.9	576	89.3
6		747	185	24.8	430	57.6	194	26.0	478	64.0		705	228	32.3	429	60.9	141	20.0	542	76.9
9		652	84	12.9	560	85.9	85	13.0	549	84.2		661	109	16.5	539	81.5	133	20.1	512	77.5
1	Sham 24 h	684	142	20.8	542	79.2	75	11.0	596	87.1	Exposed 24 h	669	196	29.3	435	65.0	122	18.2	528	78.9
3		658	229	34.8	429	65.2	74	11.2	584	88.8		674	125	18.5	538	79.8	96	14.2	571	84.7
5		645	120	18.6	471	73.0	61	9.5	575	89.1		660	188	28.5	410	62.1	96	14.5	551	83.5
6		652	143	21.9	436	66.9	136	20.9	477	73.2		667	214	32.1	363	54.4	174	26.1	435	65.2
9		687	94	13.7	523	76.1	99	14.4	558	81.2		683	128	18.7	523	76.6	133	19.5	536	78.5

Note. The numbers of nuclei studied (n_s) are given for chromosomes 1 and 10 together since double hybridization was performed. n_a and n_l are the number of asynchronous and late replication nuclei, respectively.

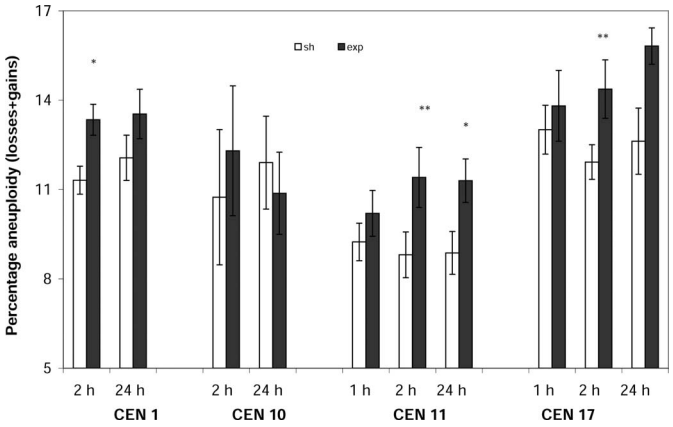

FIG. 3. Dependence of aneuploidy levels of chromosomes 11, 17, 1 and 10 on exposure duration. $n = 9$ for chromosome 11 and 17 and $n = 5$ for chromosomes 1 and 10. Error bars denote SEM. Statistical significance was determined using Tukey's HSD comparisons test. *Statistically significant at $0.03 \leq P < 0.05$; **statistically significant at $0.01 \leq P < 0.03$.

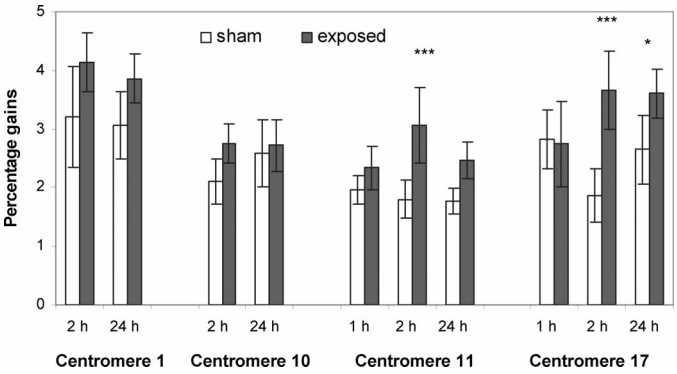

FIG. 4. Dependence of gains of chromosomes 11, 17, 1 and 10 on exposure duration. $n = 9$ for chromosomes 11 and 17 and $n = 5$ for chromosomes 1 and 10. Error bars denote SEM. Statistical significance was determined using Tukey's HSD comparisons test. *Statistically significant at $0.03 \leq P < 0.05$; **statistically significant at $0.01 \leq P < 0.03$; ***statistically significant at $P < 0.01$.

for centromere 1 ($P = 0.003$). All of the chromosomes studied (1, 10, 11 and 17) displayed statistically significant increases in the level of asynchronous replication compared with their respective sham-exposed samples after 24 h of exposure (Fig. 5). The levels in the exposed samples increased by 1.54 ± 0.46-fold for centromere 11 ($P = 0.007$), by 1.52 ± 0.54-fold for centromere 17 ($P = 0.001$), by 1.52 ± 0.18-fold for centromere 1 ($P < 0.0005$), and by 1.46 ± 0.16-fold for centromere 10 ($P = 0.011$). Only centromere 1 showed a statistically significant change in late synchronous replication at 24 h exposure ($P = 0.05$; data not shown).

DISCUSSION

The present study suggests the existence of genetic instability, reflected by increased levels of aneuploidy and increased levels of asynchronous replication of centromeres, in lymphocytes due to *in vitro* exposure to 0.1 THz CW radiation.

Genetic instability is a hallmark of cancer, manifested as either chromosomal instability leading to abnormal chromosome number (aneuploidy) or an increased mutation rate at the nucleotide level with consequent microsatellite instability (*25*). Though aneuploidy is manifested in most human cancers, it remains a subject of debate whether it is a cause or a consequence of cellular transformation (*26*). Recent reports indicate that aneuploidy can be induced in mice either by overexpression of the *MAD2* gene, an essential component of the spindle checkpoint (*27*), or by reducing the levels of centromere-link motor protein CENP-E (*28*), leading to the expression of different cancer subtypes. In addition to the genetic structural alterations that underlie the development of cancer, epigenetic mechanisms (e.g. gene silencing by DNA methylation) were also shown to be involved in the development of neoplasia (*29*). Furthermore, it was demonstrated that increased levels of aneuploidy and asynchronous replication in PBL are typical of both hematological malignancies and various solid tumors [(*14*) and references therein]. Therefore, induced genomic instability suggests the possibility of an increased risk for the development of radiation-induced cancer.

Our findings differ from previous studies where exposures were limited to 30 min or less. Scarfi *et al.* (*7*) reported no effect on the levels of micronuclei in binucleated cells after lymphocytes were exposed to 0.12 THz radiation for 20 min. In that experiment, picosecond THz pulses illuminated the target at an average power level of 1 mW and an integrated energy incidence (dose) of 0.45 J/cm^2. This dose parameter is comparable to our experiment carried out with a lower-power CW source and a longer exposure time of 2 h. However, that study used resting lymphocytes that were not induced to proliferate and used an end point that is indicative of damage incurred directly by

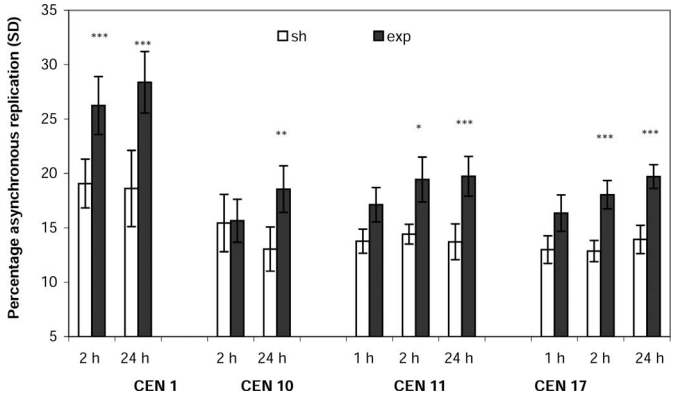

FIG. 5. Dependence of changes in asynchronous replication of the centromeres of chromosomes 11, 17, 1 and 10 on exposure duration. $n = 9$ for chromosomes 11 and 17 and $n = 5$ chromosomes 1 and 10. Error bars denote SEM. Statistical significance was determined using Tukey's HSD comparisons test. *Statistically significant at $0.03 \leq P < 0.05$; **statistically significant at $0.01 \leq P < 0.03$; ***statistically significant at $P < 0.01$.

the DNA (*7*). It should be stressed that numerical aberrations are visible only in proliferating cells. Another study found no effect of THz radiation on the activity or differentiation of primary human keratinocytes (*8*). In that experiment, pulsed THz radiation illuminated the target at an average power level of approximately 1 mW, and cells were exposed for periods of 12, 20 or 30 min, yielding total exposures of 0.15, 0.3 or 0.45 mJ/cm^2 (*8*). It should be noted that the intensity and the radiation source employed in that study are characteristic of an apparatus used in medical imaging of human skin (*8*).

When taking the increased level of aneuploidy into account, it was observed that not all chromosomes are equally affected by the radiation exposure. Chromosome 11 displayed the highest vulnerability to the THz radiation followed by chromosomes 17 and 1, with chromosome 10 displaying the least susceptibility. This is in agreement with data indicating that there is chromosome-specific aneuploidy during embryonal development (*30*) as well as in the cellular response to either chemical [metabolites (*31*)] or physical [radiation (*32*)] genotoxic insults. This specific susceptibility is also manifested after exposure to 0.8 GHz radiation (*33*).

We observed an increased level of aneuploidy after 2 h of irradiation, which was started 2 h after PHA was added. This suggests that the THz radiation induces alterations in lymphocytes that indicate a low level of cycling cells, because PHA-induced transformation of resting cells into cycling cells occurs much later (*34*). These alterations eventually lead to the observed increased level of aneuploidy. It should be noted that the exposure of the PHA-stimulated lymphocytes to radiation for 24 h occurs when a larger proportion of the cells are already cycling, leading to a comparable elevation of aneuploidy. The relationship between the exposure period and the cell cycle status of irradiated cells requires further elucidation.

It has been demonstrated previously that the induction of aneuploidy is irreversible (*14, 35*). In contrast, the epigenetic changes represented by replication timing and asynchrony that accompanied the genetic changes were reversed over time (*14, 35*). Indeed, the genetic changes reported here were accompanied by epigenetic alterations, the mechanism for interpreting the genetic information, as manifested by changes in the replication pattern of the centromeric loci, in terms both of coordinated replication and replication timing. These epigenetic modifications are even more pronounced than the changes in the aneuploidy levels after exposure to 0.1 THz radiation. All exposures led to increases in the level of asynchronous replication, which was mainly due to earlier replication, in all four centromeric loci tested, although for the shortest exposure of 1 h no statistically significant changes were observed.

As in the case of aneuploidy, we observed a difference in the effects of the exposure on the replication patterns of the different centromeres, with centromere 10 being the least ''responsive'' and showing increased SD only after 24 h while the other three centromeres were already affected after 2 h of exposure. It appears that the effects of the radiation are first observed in changes in the replication pattern, which precede changes in the level of aneuploidy. This is in agreement with findings that chromosomes whose replication is delayed display chromosomal instability (*31*).

Loss or gain of whole chromosomes leads to an imbalance in the gene dose and thus affects the expression and function not only of the genes located on the affected chromosome but also of the genes that are regulated by these genes, leading to changes in gene expression and activity (*14*).

Whatever the cause of the first aneuploid clone, it involves the unequal segregation of chromosomes during mitosis to the daughter cells (*36*). In this process the centromeric sequences play a central role [proper sister chromatid separation, metaphase mobilization and anaphase segregation (*36*)] and need to be carefully coordinated with the replicative machinery (*36*) to ensure that each DNA segment is replicated only once during each cell cycle (*36*). Thus the replication process is central to maintaining genomic stability. Indeed, our results demonstrate a positive correlation between increased levels of aneuploidy and asynchronous replication.

The major enigma regarding the mechanisms underlying biological effects of RF electromagnetic fields is whether the RF-field-induced biological response is due to thermal or non-thermal effects. The possibility of affecting cellular processes through non-thermal effects has been at the center of a major dispute for several years when considering exposure hazards to electromagnetic radiation in the spectral range of radiofrequency. It should be pointed out that the international guidelines are based on preventing short-term, immediate health effects such as stimulation of peripheral nerves and muscles or elevation of tissue temperatures by more than 1°C as a result of absorption of energy during exposure (*37, 38*). Therefore, we have examined whether significant temperature elevation can occur after exposure to the power density used in our experiment.

The power density in our cell samples, which consisted of a very thin layer of lymphocytes (~0.003 cm) at the bottom of a 0.2-cm-deep layer of high culture medium, has been calculated to be 0.031 mW/cm^2. This value is 160-fold lower than the limit of 5 mW/cm^2 set for occupational exposure and 30-fold lower than the limit of 1 mW/cm^2 set for the general population (*37, 38*). Moreover, no macroscopic steady-state temperature elevation within the 0.1-cm layer at the bottom of the culture flask could be detected by optics-based temperature sensors within an experimental accuracy of ±0.2°C. We previously showed that the levels of both asynchronous replication and aneuploidy of chromosome 17 were not altered by temperature changes in the range of 34.5–39.5°C (*39*). Therefore, even if a microscopic transient elevation of temperature does take place, it cannot be responsible for the observed increase in genomic instability.

The nature of the primary mechanism(s) underlying the 0.1 THz radiation-induced increase in genomic instability is unknown at this stage. It may be speculated, based on THz spectroscopy of proteins and DNA in the range of 0.1–10 THz, that this radiation is able to excite low-frequency collective vibrational modes of biomolecules (*6*). In the case of DNA molecules, these low vibrational modes consist of molecular internal vibrations such as twisting, bending and stretching of the double helix, sugar pseudorotational vibrations and fluctuations of the weakest bonds or non-bonded interactions [van der Waals forces, dispersion forces, and hydrogen bonding (*40–43*)]. The internal motions, which depend on the weak hydrogen bonds of the double-helix base pairs (*44*), are extremely sensitive to DNA composition and topology and thus may have a negative impact on the reliability of replication process.

From our results, we can surmise that the 0.1 THz radiation constitutes an insult to the replication machinery of the lymphocytes *in vitro*, which leads to increased levels of aneuploidy. Thus, while ICNIRP concluded that the available data are insufficient to provide a basis for setting exposure restrictions (*37*) in the case of potential long-term effects of exposure such as an increased risk of cancer, based on our results, it may be proposed that relatively long exposure to the low power density of 0.1 THz radiation may lead to an increased risk for the development of cancer. Further work is needed to elucidate the relationship between the induced genomic instability *in vitro* and the risk for malignant transformation *in vivo.*

ACKNOWLEDGMENTS

This work was carried out with financial support from the Commission of the European Communities, specific RTD program ''Quality of Life and Management of Living Resources'', QLK4-2000-00129 (''THz Bridge''). Partial support of the radiation source was provided by the Israeli Ministry of Science and Technology. This work is based on a portion of a dissertation submitted by P. Hasin in partial fulfillment of the requirements for the MSc degree to Tel-Aviv University.

Received: January 3, 2007; accepted: March 12, 2008

REFERENCES

1. J. F. Federici, B. Schulkin and F. Huang, THz imaging and sensing for security applications—explosives, weapons and drugs. *Semiconductors Sci. Tech.* **20**, S266–S280 (2005).
2. E. Berry, J. W. Handley and A. J. Fitzgerald, Multispectral classification techniques for terahertz pulsed imaging: an example in histopathology. *Med. Eng. Phys.* **26**, 423–430 (2004).
3. T. Kleine-Ostmann, K. Pierz, G. Hein, P. Dawson and M. Koch, Audio signal transmission over THz communication channel using semiconductor modulator. *Elect. Lett.* **40**, 124–126 (2004).
4. G. Markelz, A. Roitberg and E. J. Heilweil, Pulsed terahertz spectroscopy of DNA, bovine serum albumin and collagen between 0.1 and 2.0 THz. *Chem. Phys. Lett.* **320**, 42–48 (2000).
5. P. Woolard, P. Zhao and H. L. Cui, THz-frequency intrinsic oscillations in double-barrier quantum well systems. *Phys. B Condens. Matter* **314**, 108–112 (2002).
6. R. Globus, D. L. Woolard and T. Khromova, THz-spectroscopy of biological molecules. *J. Biol. Phys.* **29**, 89–100 (2003).
7. R. Scarfi, M. Romano and R. Di Pietro, THz exposure of whole blood for the study of biological effects on human lymphocytes. *J. Biol. Phys.* **29**, 171–177 (2003).
8. R. H. Clothier and N. Bourne, Effects of THz exposure on human primary keratinocyte differentiation and viability. *J. Biol. Phys.* **29**, 179–185 (2003).
9. A. Doria, G. P. Gallerano, E. Giovenale, G. Messina, A. Lai, A. Ramundo-Orlando, V. Sposato, M. D'Arienzo, A. Perrotta and O. Zeni, THz radiation studies on biological systems at the ENEA FEL facility. *Infrared Phys. Tech.* **45**, 339–347 (2004).
10. M. Feychting, A. Ahlborn and L. Kheifets, EMF and health. *Annu. Rev. Pub. Health* **26**, 165–189 (2005).
11. P. Duesberg and R. Li, Multistep carcinogenesis: a chain reaction of aneuploidizations. *Cell Cycle* **2**, 202–210 (2003).
12. P. A. Jones, Overview of cancer epigenetics. *Semin. Hematol.* **42**, S3–S8 (2005).
13. L. A. Loeb, Mutator phenotype may be required for multistage carcinogenesis. *Cancer Res.* **51**, 3075–3079 (1991).
14. A. Korenstein-Ilan, A. Amiel, S. Lalezari, M. Lishner and L. Avivi, Allele-specific replication associated with aneuploidy in blood cells of patients with hematologic malignancies. *Cancer Genet. Cytogenet.* **139**, 97–103 (2002).
15. M. Fukuda and A. Sun, The DNA-instability test as a specific marker of malignancy and its application to detect cancer clones in borderline malignancy. *Eur. J. Histochem.* **49**, 11–26 (2005).
16. S. Gagos and I. Irminger-Finger, Chromosome instability in neoplasia: Chaotic roots to continuous growth. *Int. J. Biochem. Cell Biol.* **37**, 1014–1033 (2005).
17. O. M. Sieber, K. Heinimann and I. P. Tomlinson, Genomic instability—the engine of tumorigenesis? *Nat. Rev. Cancer* **3**, 701–708 (2003).
18. S. Henikoff and Y. Dalal, Centromeric chromatin: what makes it unique? *Curr. Opin. Genet. Dev.* **15**, 177–184 (2005).
19. S. Selig, K. Okumura, D. C. Ward and H. Cedar, Delineation of DNA-replication time zones by fluorescence *in situ* hybridization. *EMBO J.* **11**, 1217–1225 (1992).
20. B. Mukherjee, V. V. V. S. Murty and R. S. K. Chaganti, Detection of cell-cycle stage by fluorescence *in situ* hybridization—Its application in human interphase cytogenetics. *Cytogenet. Cell Genet.* **61**, 91–94 (1992).
21. R. L. Abrams, Coupling losses in hollow waveguide laser resonators. *IEEE J. Quantum Electron.* **8**, 838–843 (1972).
22. A. Yariv, *Optical Electronics in Modern Communications* in *Oxford series in Electrical and Computer*, 5th ed. Oxford University Press, New York, 1997.
23. J. T. Kindt and C. A. Schmuttenmaer, Far-infrared dielectric properties of polar liquids probed by femtosecond tetrahertz pulse spectroscopy. *J. Phys. Chem.* **100**, 10373–10379 (1996).
24. M. G. Brown and J. H. Lawce, In *The AGT Cytogenetics Laboratory Manual* (M. J. Barch, T. Knutsen and J. L. Spurbeck, Eds.), pp. 77–172. Lippincott-Raven, Philadelphia, PA, 1997.
25. D. P. Cahill, C. Lengauer, J. Yu, G. J. Riggins, J. K. V. Willson, S. D. Markowitz, K. W. Kinzler and B. Vogelstein, Mutations of mitotic checkpoint genes in human cancers. *Nature* **392**, 300–304 (1998).
26. D. Pellman, Aneuploidy and cancer. *Nature* **446**, 38–39 (2007).
27. R. Sotillo, E. Hernando, E. Díaz-Rodríguez, J. Teruya-Feldstein, C. Cordón-Cardo, S. W. Lowe and R. Benezra, Mad2 overexpression promotes aneuploidy and tumorigenesis in mice. *Cancer Cell* **11**, 9–23 (2007).
28. B. A. A. Weaver, A. D. Silk, C. Montagna, P. Verdier-Pinard and D. W. Cleveland, Aneuploidy acts both oncogenically and as a tumor suppressor. *Cancer Cell* **11**, 25–36 (2007).
29. A. H. Ting, K. M. McGarvey and S. B. Baylin, The cancer epigenome—components and functional correlates. *Genes Dev.* **20**, 3215–3231 (2006).
30. S. Munne, M. Bahce, M. Sandalinas, T. Escudero, C. Marquez, E. Velilla, P. Colls, M. Oter, M. Alikani and J. Cohen, Differences in

chromosome susceptibility to aneuploidy and survival to first trimester. *Reprod. Biomed. Online* **8**, 81–90 (2004).

31. L. Zhang, W. Yang, A. E. Hubbard and M. T. Smith, Nonrandom aneuploidy of chromosomes 1, 5, 6, 7, 8, 9, 11, 12, and 21 induced by the benzene metabolites hydroquinone and benzenetriol. *Environ. Mol. Mutagen.* **45**, 388–396 (2005).

32. K. S. Breger, L. Smith, M. S. Turker and M. J. Thayer, Ionizing radiation induces frequent translocations with delayed replication and condensation. *Cancer Res.* **64**, 8231–8238 (2004).

33. R. Mazor, A. Korenstein-Ilan, A. Barbul, Y. Eshet, A. Shahadi, E. Jerby and R. Korenstein, Increased levels of numerical chromosome aberrations after *in vitro* exposure of human peripheral blood lymphocytes to radiofrequency electromagnetic fields for 72 hours. *Radiat. Res.* **169**, 28–37 (2008).

34. Y-C. Kuo, N-S. Yang, C-J. Chou, L-C. Lin and W-J. Tsai, Regulation of cell proliferation, gene expression, production of cytokines, and cell cycle progression in primary human T lymphocytes by piperlactam S isolated from *Piper kadsura*. *Mol. Pharmacol.* **58**, 1057–1066 (2000).

35. A. Nagler, A. Korenstein-Ilan, A. Amiel and L. Avivi, Granulocyte colony-stimulating factor generates epigenetic and genetic alterations in lymphocytes of normal volunteer donors of stem cells. *Exp. Hematol.* **32**, 122–130 (2004).

36. D. Y. Takeda and A. Dutta, DNA replication and progression through S phase. *Oncogene* **24**, 2827–2843 (2005).

37. ICNIRP, Guidelines for limiting exposure to time-varying electric, magnetic, and electromagnetic fields (up to 300 GHz) *Health Phys.* **74**, 494–522 (1998).

38. NCRP, *Biological Effects and Exposure Criteria for Radiofrequency Electromagnetic Fields.* Report 86, National Council on Radiation Protection and Measurements, Bethesda, 1986.

39. M. Mashevich, D. Folkman, A. Kesar, A. Barbul, R. Korenstein, E. Jerby and L. Avivi, Exposure of human peripheral blood lymphocytes to electromagnetic fields associated with cellular phones leads to chromosomal instability. *Bioelectromagnetics* **24**, 82–90 (2003).

40. W. N. Mei, M. Kohli, E. W. Prohofsky and L. L. Van Zandt, Acoustic modes and nonbonded interactions of the double helix. *Biopolymers* **20**, 733–752 (1981).

41. L. Young, V. V. Prabhu and E. W. Prohovsky, Calculation of far-infrared absorption in polymer DNA. *Phys. Rev. A* **39**, 3173–3180 (1989).

42. Y. Feng and E. W. Prohofsky, Vibrational fluctuations of hydrogen bonds in a DNA double helix with nonuniform base pairs. *Biophys. J.* **57**, 547–553 (1990).

43. D. H. Lin, A. Matsumoto and N. Go, Normal mode analysis of a double-stranded DNA dodecamer d(CGCGAATTCGCG). *J. Chem. Phys.* **107**, 3684–3690 (1997).

44. T. Weidlich, S. M. Lindsay, W. L. Peticolas and G. A. Thomas, Low-frequency raman-spectra of z-DNA. *J. Biomol. Struct. Dyn.* **7**, 849–858 (1990).